

SPECIAL ISSUE PAPER

Channel response to sediment replenishment in a large gravel-bed river: The case of the Saint-Sauveur dam in the Buëch River (Southern Alps, France)

Guillaume Brousse¹  | Gilles Arnaud-Fassetta¹ | Frédéric Liébault²  | Mélanie Bertrand² | Gabriel Melun³ | Remi Loire⁴  | Jean-René Malavoï⁴ | Guillaume Fantino⁵ | Laurent Borgniet⁶

¹UMR 8586 (PRODIG), Université Paris-Diderot (Paris 7), Paris, France

²Irstea, ETNA, University of Grenoble Alpes, Grenoble, France

³DREC, Agence Française pour la Biodiversité (AFB), Vincennes, France

⁴DPIH/CIH, EDF, Lyon, France

⁵GEOPEKA, Lyon, France

⁶Irstea, LESSEM, University of Grenoble Alpes, Grenoble, France

Correspondence

G. Brousse, Université Paris-Diderot (Paris 7), UMR 8586 (PRODIG), Paris 75013, France.
Email: guillaume.brousse@univ-paris-diderot.fr

Funding information

Agence française pour la biodiversité; Électricité de France; INTERREG Alpine Space HyMoCARES

Abstract

The Saint-Sauveur dam was built in 1992 in the middle section of the Buëch River. Downstream of the dam, a channel incision by several meters was observed. A gravel replenishment operation was planned in order to restore the active channel. An equivalent of two times the mean annual bedload-transport capacity (43,500 m³) was replenished downstream of the dam in September 2016. The aim of this paper is to quantify morphological change associated with sediment remobilization in order to evaluate the efficiency of the restoration works. The monitoring was based on a combination of (a) change detection using sequential high-resolution digital elevation models (from airborne LiDAR data), (b) bedload tracing using active ultrahigh-frequency radio-frequency identification technology, and (c) complementary field surveys of channel grain-size distribution and morphology for bedload-transport computation. Field monitoring allows us to capture a net aggradation along a 2-km reach after the first post-replenishment flood. A sediment balance analysis was performed to back-calculate bedload supply coming from the sluicing operation during the flood. Although the sediment replenishment operation clearly had a positive impact on the morphological conditions of the starved river reach, the effective bedload supply from artificial berms (22,650 m³) was insufficient to initiate substantial channel shifting along the restored reach and a subsequent amplification of the sediment recharge. The combination of high-resolution topographic resurveys and sediment tracing was successful to evaluate the downstream propagation of sediment replenishment effects.

KEYWORDS

braided river, dam impact, restoration, river management, sediment replenishment

1 | INTRODUCTION

The sediment budget of many Alpine rivers was strongly impacted by the cumulative effects of different anthropogenic actions linked to

valley development during the last decades, leading to a global trend of sediment deficit (e.g., Surian & Rinaldi, 2003; Piégay, Alber, Slater, & Bourdin, 2009; Liébault, Lallias-Tacon, Cassel, & Talaska, 2013). The causes of disturbance are clearly recognized: (a) gravel mining in active

channels; (b) river regulation; and (c) dam construction. In parallel, a general decrease of sediment supply from headwaters was observed and was particularly well documented in the Southern French Alps, where it has been attributed to several environmental changes: (a) climate change following the end of the Little Ice Age; (b) spontaneous reforestation following rural depopulation; and (c) torrent-control works during the 1860–1915 period (e.g., Astrade, Jacob-Rousseau, Bravard, Allignol, & Simac, 2011; Liébault et al., 2005; Liébault & Piégay, 2002). In this context, sediment continuity was temporally broken or strongly modified, and bed incision and channel pattern shift from braided to single-thread styles were observed along many Alpine rivers. These sediment-related alterations not only have direct consequences on infrastructures like bridges, dikes, or roads but also induce a dramatic loss of aquatic habitats (e.g., Belletti, Dufour, & Piégay, 2013; Bravard et al., 1997).

Sediment replenishment (or gravel augmentation) is one of the possible solutions for compensating sediment deficit downstream of dams and for restoring aquatic habitats of starved river channels (e.g., Habersack & Piégay, 2008; Kondolf et al., 2014; Sumi, 2006; USDA, 2004). This operation consists in artificially injecting coarse sediment in active channels downstream a dam, in such a way that those materials can be easily removed and transported during high-frequency floods. Sediments are generally deposited by creating berms, which are expected to be scoured during floods. According to Ock, Sumi, and Takemon (2013), four methods of replenishment are commonly used: (a) in-channel bed stockpile; (b) high-flow stockpile; (c) point-bar stockpile; and (d) high-flow direct injection. According to Sklar et al. (2009), the efficiency of replenishment can be evaluated by the resultant extension and duration of riverbed morphological change, which depends on the dispersive or translational nature of the generated sediment pulses.

This type of sediment management downstream of dams is common in Japan (e.g., Kantouch, Sumi, Kubota, & Suzuki, 2010; Musashi, Nakata, Suzuki, Oshima, & Demizu, 2016; Okano, Kikui, Ishida, & Sumi, 2004; Sakurai & Hakoishi, 2013) and in the United States (e.g., Kondolf et al., 2007; Kondolf & Minear, 2004; Merz, Pasternack, & Wheaton, 2006; Wheaton, Pasternack, & Merz, 2004) but it is less frequent in Europe where only few cases are known (e.g., Arnaud et al., 2017). Replenishment with coarse sediments in the Alpine context is an engineering challenge because of the lack of feedback reporting from few field experiments and the subsequent difficulties to anticipate project efficiency. Only two case studies in Alpine gravel-bed rivers have been reported (Arnaud et al., 2017; Heckmann, Haas, Abel, Rimböck, & Becht, 2017), highlighting the difficulty to isolate the morphological effects of sediment replenishment and the importance of the reinjected volume for restoration efficiency. Furthermore, sediment replenishment has been recently investigated through flume experiments and numerical modelling in order to compare different designs of sediment reinjection in river channels. The flume experiments by Battisacco, Franca, and Schleiss (2016) and the numerical modelling by Juez, Battisacco, Schleiss, and Franca (2016) showed that the placement of several berms on both sides of the channel, in a parallel

configuration and under conditions of complete submersion, is the best condition for a maximum erosion efficiency.

The main goal of the study is to investigate the morphological effect of sediment replenishment in a large gravel-bed river using an intensive field-based monitoring approach. Explored scientific issues are (a) the quantification of effective bedload supply from berm erosion during a flood in a context of high-flow stockpile design of gravel replenishment, (b) the detection of the sediment wave propagation following a flood event, and (c) the characterization of the morphological effects of the sediment wave along a degrading wandering channel.

A major sediment replenishment operation was recently implemented in the Buëch River (Southern French Alps; Figure 1a) downstream of the Saint-Sauveur dam to stop channel incision and restore aquatic habitats of an altered, large braided channel. This field experiment of one-shot gravel reinjection downstream of a large dam is the largest ever done in Alpine rivers in terms of single reintroduced volume, and it provides a unique opportunity to investigate the morphological effect of such mitigation actions (sediment continuity and sediment balance recovery). The occurrence of a 5-year flood few weeks after the replenishment during which hydraulic sluicing was operating gave the opportunity to evaluate the replenishment efficiency by looking not only at the amount of the reinjected volume, which effectively fed the starved river reach, but also at the downstream propagation of the generated sediment pulse.

2 | STUDY SITE

The Buëch, a gravel-bed braided river draining the Southern French Prealps, is a major Alpine tributary (Rank 5, Strahler) of the Durance River (Rank 6 at the confluence of Sisteron). The Saint-Sauveur dam is located 4 km downstream of the city of Serres (Figure 1b). This dam drains an 836-km² upland watershed with a maximum elevation of 2,709 m asl. The watershed geology is exclusively represented by sedimentary rocks, with alternating folded sequences of marls and limestones. The climate is Mediterranean, with a mean annual rainfall of ~800 mm. The mean daily discharge at the Serres gauging station located upstream of the dam (1964–2014) is 14.1 m³ s⁻¹, and the 2-, 5-, 10-, and 50-year daily flood discharges are estimated at 140, 210, 250, and 350 m³ s⁻¹, respectively.

The study reach (6.85 km long) extends from the Saint-Sauveur dam down to the bridge of Eyuans (Figure 1c). We distinguished three different hydromorphological unit (HUMs) expressed in length (*L*), area (*A*), and width (*W*): HUM1 (*L*, 0.55 km; *A*, 5.44 ha; *W*, 85 m) corresponds to the replenishment site; HUM2 (*L*, 2 km; *A*, 30.79 ha; *W*, 63 m) corresponds to the most altered reach; and HUM3 (*L*, 4.3 km; *A*, 101.5 ha; *W*, 166 m) is a more preserved braided channel. The whole study reach presents a mean active-channel width of 130 m and a mean channel slope ranging from 0.006 to 0.009 m m⁻¹. The channel morphology is a succession of segments characterized by wandering and braided patterns, although this reach is included in a ~1-km-wide alluvial floodplain. The lateral confinement related to roads or bedrock outcrops is important. Well-preserved patches of alluvial forests are only observed in the left side of the channel

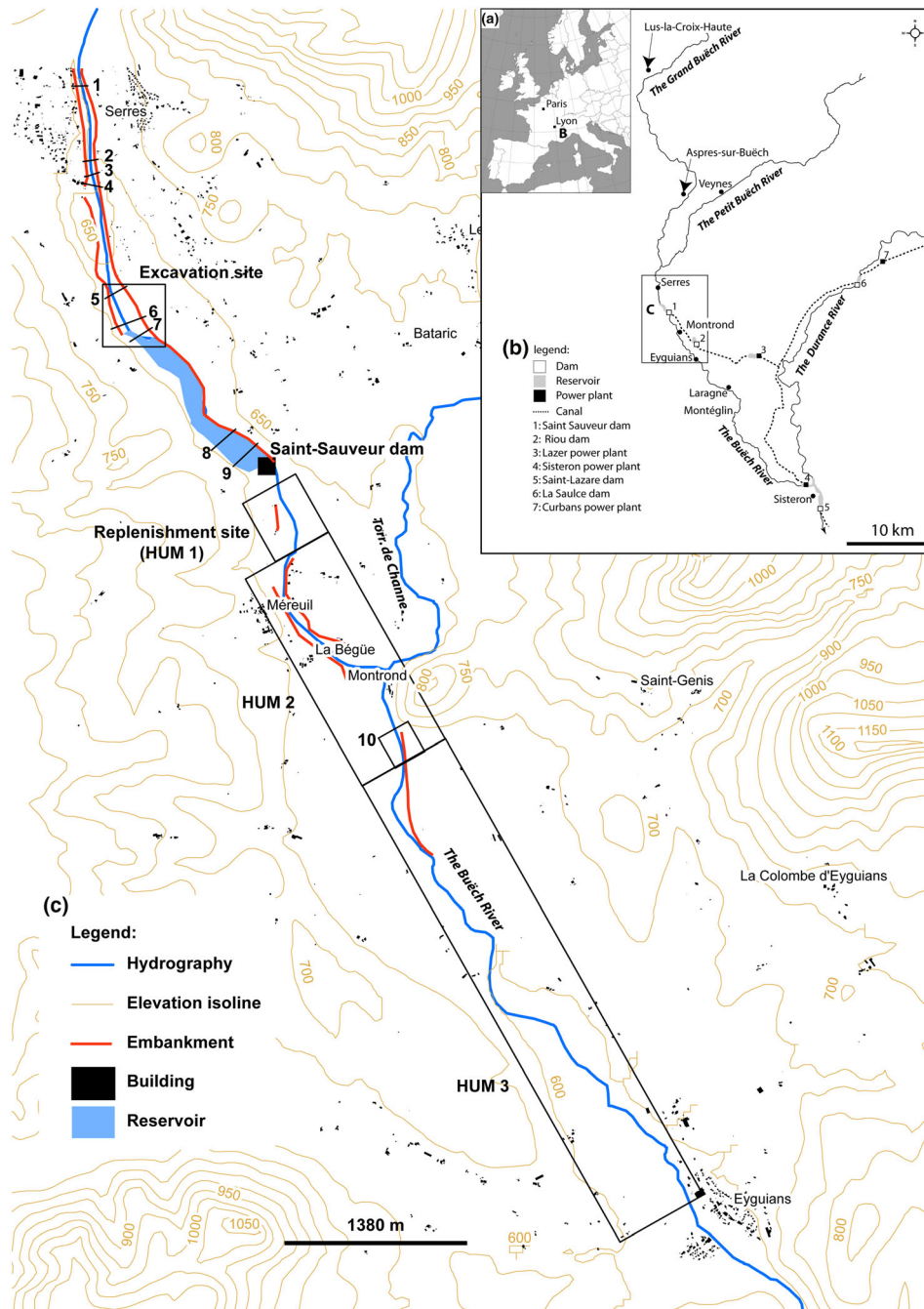


FIGURE 1 Location of the study site. (a) Location of the Buëch River in Western Europe. (b) Location of the study site in the Durance hydraulic power plant network. (c) Sectorization of the study reach. 1 to 9, radio-frequency identification tag injection transects; 10, study reach for bedload-transport computation [Colour figure can be viewed at wileyonlinelibrary.com]

immediately downstream from the dam and in the right-side downstream of the confluence with the Torrent de Channe. Most of the floodplain is occupied by cultivated lands and grasslands.

3 | WHY AND HOW A SEDIMENT REPLENISHMENT IN THE BUËCH RIVER AT SAINT-SAUVEUR?

The Buëch River has been highly impacted by intensive gravel mining since the late 1960s until 2012 (e.g., Gautier, 1994; Liébault

et al., 2013). The total volume of gravel extracted from three active mining sites was estimated between 5 and 9.7 Mm³ (e.g., HYDRÉTUDES, 2013). In addition to gravel mining, the bedload-transport continuity was strongly impacted by the construction of the Saint-Sauveur dam. This 10-m-high and 260-m-wide barrier was constructed between 1990 and 1991 by EDF (French power plant company), and the commissioning started in 1992. The construction required dredging of 600,000 m³ of sediment. The full storage capacity of the reservoir is 1.72 Mm³, and the water is used for irrigation, hydroelectricity, and touristic development. The dam

serves as a water intake structure, supplying a diversion canal, with a maximum hydraulic capacity of $30 \text{ m}^3 \text{ s}^{-1}$, conducting water to the laser hydropower plant located 10 km downstream. Downstream of the dam, the hydrological regime is strongly regulated at 1/10 of the mean interannual discharge. This global annual volume is redistributed along seasons for aquatic habitat at $0.9 \text{ m}^3 \text{ s}^{-1}$ between July and September, at $1.5 \text{ m}^3 \text{ s}^{-1}$ during late June and early October, at $2 \text{ m}^3 \text{ s}^{-1}$ between mid-October and early March, and at $2.5 \text{ m}^3 \text{ s}^{-1}$ between early March and mid-June. Although the Saint-Sauveur dam is equipped with three flood gates, allowing some sediment transport continuity during floods (sluicing operations), most of the coarse sediments are trapped in the proximal part of the reservoir. It has been estimated that only $20,000 \text{ m}^3$ of the yearly coarse sediment load ($42,000 \text{ m}^3$) could be transported through the dam (e.g., HYDRÉTUDES, 2013). This dam has been classified by EDF as partially transparent to the coarse sediment transport in term of volume, grain size, and frequency (Loire, 2018), a situation corresponding to 20% of EDF dams.

These alterations of sediment regime may have been amplified by the general context of sediment supply decrease from the watershed and the resulting significant channel responses, that is, active-channel narrowing and channel degradation, as attested by the historical long profile of 1908 (Liébault et al., 2013). A shift from a braided to wandering pattern can be clearly observed along HUM1 and HUM2. Downstream of the dam, the channel incision reaches 3 m few years after dam construction and propagates downstream

(HYDRÉTUDES, 2013). Some marly bedrock outcrops are observed along the degraded reach, as well as undercut groynes on the right bank.

In September 2016, EDF artificially increased the coarse sediment supply to the reach. The replenishment operation consisted in the reintroduction of $43,500 \text{ m}^3$ of gravel downstream of the dam. This volume was constrained by the flood risk management plan of the Departmental Direction of the Territories (DDT 05), which imposes a bed level not to be exceeded in the replenishment reach. Sediments were directly excavated from the alluvial fan deposited in the reservoir. This sediment volume represents two times the estimated mean annual bedload yield crossing the dam. Gravels were deposited along HUM1 by the creation of two artificial gravel berms according to the “high-flow stockpile method” (Ock et al., 2013; Figure 2a). The relative elevation of berms above the bed level ranges from 1.3 to 2.8 m, and therefore, these surfaces are not submerged during frequent floods (Figure 2b). Berms were composed of two different parallel units (BU): the $12,300 \text{ m}^3$ right berm unit (BU1; 190 m long; 31 m wide; 1/7 bank slope) and the $31,200 \text{ m}^3$ left berm unit (BU2; 360 m long; 46 m wide; 2/3 bank slope). The grain-size distribution (GSD) of berms was obtained by bulk sampling ($D_{50} = 33 \text{ mm}$, $D_{84} = 86.3 \text{ mm}$, and $D_{90} = 102 \text{ mm}$) in the alluvial fan where the sediment has been excavated and is therefore representative of the bedload GSD of the Buëch River. In addition, a trench was cut into the left berm (380 m long; 6.5 m wide; 2/3 bank slope) in order to facilitate the remobilization of an alluvial terrace, which was part of

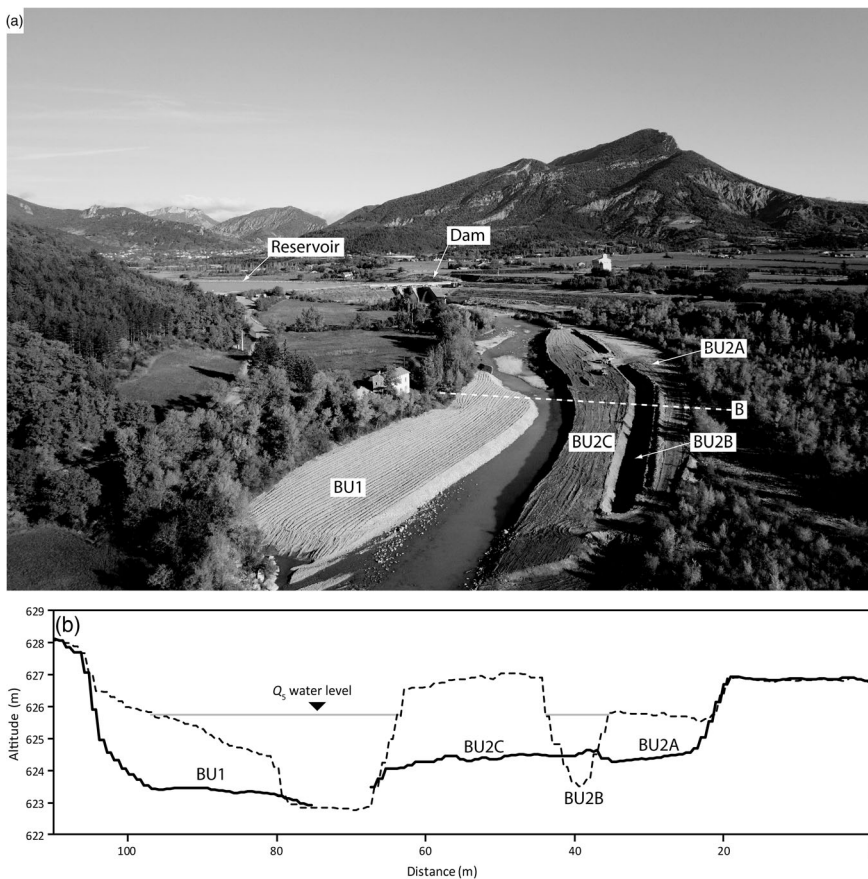


FIGURE 2 Artificial gravel replenishment downstream of Saint-Sauveur dam in the Buëch River. (a) Unmanned aerial vehicle view looking upstream (October 22, 2016, 10:33 a. m.). (b) Typical cross section. The dark line represents the initial cross section (February 2015), and the dashed line represents the postreplenishment cross section (November 2016)

the active channel before dam construction and to avoid right-bank channel shifting in marly bedrock outcrops. The trench divided BU2 in three subunits: the left side of the left berm (BU2A), the trench (BU2B), and the right side of the left berm (BU2C). In order to maximize the efficiency of the project, the power plant company modified dam exploitation by increasing the number and duration of sluicing (opening flood gates and reduce reservoir level until supercritical conditions recovery) during floods.

4 | METHODS

The physical monitoring combines a bedload tracing programme using active ultrahigh-frequency radio-frequency identification (RFID) technology, a repetitive high-resolution topographic survey of the restored reach, and ancillary field surveys for specific data analysis (e.g., bedload-transport computation).

4.1 | Bedload tracing programme

A bedload tracing programme was implemented to evaluate the sediment transparency (or bedload trapping efficiency) of the Saint-Sauveur dam and to monitor the bedload dispersion along the restored reach. Artificial cobbles and pebbles equipped with active ultrahigh-frequency RFID tags (COIN ID; 433.92 MHz; $n = 148$) were injected upstream of the dam in November 2016 along nine cross sections (Figure 1c). It was also planned to inject tracers into berms, but the first post-restoration flood occurs too rapidly to have time to deploy them. Cross sections were equipped with 16 tracers except for the two last that were equipped with 18 tracers. Patches of artificial tracers were placed at regular intervals along cross sections; they replicate natural imbrication and correctly represent the form and density of natural cobbles-pebbles of the site (Table 1). Because the size of RFID tags limits the minimum b -axes of tracer at 32 mm, our observations of bedload dispersion are limited to the coarser part (i.e., above the D_{50}) of the bedload GSD. Active tags allowed us to detect artificial cobbles and pebbles in surface (range of 80 m according to ELA Innovation©), in subsurface, and below water (e.g.,

TABLE 1 Characteristics of artificial cobbles-pebbles equipped with active RFID tags

Artificial cobbles-pebbles characteristics	Grain size (in mm)		
	32–45	45–64	64–90
Number of tracers	43	70	35
A-axis (mm)	53–75	85–94	94–105
B-axis (mm)	38–44	51–61	72–87
C-axis (mm)	37–40	48–49	59–62
Weight (g)	146–228	296–377	513–766
Volume (cm ³)	54–85	111–140	195–288
Density	2.69	2.67–2.69	2.63–2.66

Abbreviation: RFID, radio-frequency identification.

Cassel, Dépret, & Piégay, 2017). Active tags have smaller lifetime than passive ones, but there is no signal collision, and each tag can be detected even when they are very close to each other (Piégay, Cassel, Dépret, Michel, & Rollet, A.-J., & Vaudor, L., 2016). Tracer inventories were done in late January 2017 along wadable portions of the channel, and in early February 2017 by craft along nonwadable areas.

4.2 | Repetitive high-resolution topographic surveys

Repetitive topographic surveys of the restored reach were obtained from two high-resolution digital elevation models (4 pixels m⁻²) derived from sequential airborne LiDAR surveys. Technical specifications of the two LiDAR surveys are very similar (Table 2) and water discharges downstream of the dam were strictly the same during the two surveys. Global precision of LiDAR data was measured on immobile targets on three different sites by the private company in charge of LiDAR data acquisition. The root mean square error of z values are 0.020 and 0.063 m for the first and second LiDAR surveys, respectively. Topographic data include only emerged surface. In addition, sufficient numbers of echoes are recorded in water surface and allow us to interpolate them in each baseflow channel. The low water discharges during the two surveys indicate that the submerged portions of the active channel were spatially limited during data acquisition and may not have a substantial effect on calculated erosion

TABLE 2 Technical specifications of airborne LiDAR data acquisitions

Characteristics	LiDAR1	LiDAR2
Date	November 4, 2016	December 22, 2016
Laser	Riegl LMS Q680i	
Flight height (m above ground level)	500	
Flight speed (in nd)	60	
Scan frequency (kHz)	400	
Altimetric accuracy (m)	0.1	
Planimetric accuracy (m)	0.1	0.25
Point density (point/m ²) ^a	16–72	17–60
Ground control points	42	129
Mean error (m)	–0.003	0.018
RMSE (m)	0.02	0.06
Discharge upstream of the dam (m ³ s ⁻¹)	1.7	7.1
Regulated discharge (m ³ s ⁻¹) ^b	2	
Water release (m ³ s ⁻¹) ^c	0	

Abbreviation: RMSE, root mean square error.

^aPoint density after filtering vegetation and water echoes.

^bMinimum discharge downstream of the dam according to dam exploitation rules (e-flow).

^cDifference between natural discharge upstream of the dam, diverted water, and regulated discharge.

and deposition volumes. However, computed gross volumes of erosion and deposition must be considered as lower bound estimates of the true values.

A control of the alignment between the two surveys was done using the 3D point clouds, following the procedure described by Lallias-Tacon, Liébault, and Piégay (2014). Stable areas well distributed along the study reach floodplain in which land use has not changed (garden, grassland, and road) were selected in order to evaluate the systematic error in elevation (σ_{sys}). A mean error (ME) of -0.028 m was obtained in a set of 7,869 random single points and confirm the presence of a significant systematic error. A realignment of the two point-clouds using the CloudCompare software was done to reduce the systematic error. We fix the first LiDAR, as the reference and stable areas were extracted on each cloud in order to calculate the 3D correction matrix. This latter was used to realign the second survey. Realignment decreases ME from -0.028 to 0.0015 m, which confirms realignment necessity. Digital elevation model of difference (DoD) was used to calculate elevation change separately on HUM1, HUM2, and HUM3. Two types of volumetric calculations were distinguished: (a) gross erosion or gross deposition volumes and (b) net sediment balance. According to Anderson (2019), gross volumes necessitate a thresholding but not net volumes. A threshold of 0.129 m was obtained by computing the level of detection (LoD) of significant elevation change (95% confidence interval) calculated by $\text{LoD} = 1.96\sigma_z$ with $\sigma_z = \left(\text{RMSE}_{\text{LIDAR1}}^2 + \text{RMSE}_{\text{LIDAR2}}^2 \right)^{0.5}$ according to Lane, Westaway, and Murray (2003). LoD was subtracted from the DoD and then excluded according to the Carley et al. (2012) method. Gross and net volume uncertainty (σ_v) was estimated using the error model of Anderson (2019) that accounted for systematic errors and spatially correlated random errors:

$$\sigma_v = nL2 \sqrt{\frac{\sigma_{\text{sc}}^2 \pi a_i^2}{n 5L^2} + \sigma_{\text{sys}}}, \quad (1)$$

with n is the number of cells outside LoD interval, L the cell size, and a_i the range over which errors were correlated. The magnitude of the spatially correlated random errors (σ_{sc}) was obtained by semivariogram analysis in unvegetated stable surfaces and new set of 13,142 random single points. Systematic errors (σ_{sys}) were given by the ME after realignment process. Cross sections were extracted from the DoD every 50 m with a spatial resolution of 1 m in order to reconstruct the longitudinal bed-level evolution. The downstream evolution of the low-flow channel (water surface) was obtained by extracting the minimum elevation of the cross section (Z_{min}). The downstream evolution of the active-channel elevation was obtained by calculating the mean elevation of the cross section (Z_{cs}).

In order to compare our results with other case studies, we choose a set of metrics inspired by Battisacco et al. (2016). Berm erosion was evaluated by the persistence of sediment replenishment (PR in %), which illustrates the volume not remobilized by the flow:

$$\text{PR} = \left(1 - \frac{\text{ER}}{R} \right) 100, \quad (2)$$

with ER is the effective replenishment eroded volume (in m^3) and R the replenished volume (in m^3). We used each cross section of HUM1 in order to quantify the eroded width by calculating the width ratio (WR):

$$\text{WR} = \left(1 - \frac{\sum W_e}{\sum W_b} \right) 100, \quad (3)$$

with W_e is the eroded width (in m) and W_b the berm width (in m). WR illustrates the relative undisturbed width for each cross section and separately for each berm unit. The magnitude of the morphological impact was appreciated by the length of bed aggradation (LR) in the downstream reach:

$$\text{LR} = \frac{L}{L_b}, \quad (4)$$

with L is the length of the aggraded reach (in m) and L_b the maximum berm length (in m). LR is used to qualify replenishment efficiency. Submergence of each berm unit has been appreciated by photo analysis at the peak flow.

4.3 | Ancillary field surveys and bedload-transport computation

Bedload transport was computed according to the GTM model (Generalized Threshold Model; Recking, 2016) in order to estimate the coarse sediment output in the study reach and to close the sediment balance associated with the flow event. This computation was based on data collected in the field. The study reach for bedload computation was located at the downstream end of HUM2 (Figure 1b). A cross section of the active channel and the channel slope along a distance of 346 m were surveyed using a level and a rod. In a band of 10–20 m along the cross section, each flood mark was characterized with a z value. Flood-mark projection along the cross section allows us to evaluate the mean depth (d) during high flow and compute the hydraulic radius for Q_{max} . The surficial GSD was obtained by a classic pebble count (Wolman, 1954) sampling of 200 particles on a lateral bar on the right bank of the cross section ($D_{50} = 20.8$ mm; $D_{84} = 40.9$ mm). A channel slope of 0.0032 m m^{-1} was obtained.

Critical adimensional shear stress for the bed D_{84} ($\tau_{\text{c}84}^* = 0.56 S + 0.021$, with S as the channel slope in m m^{-1}) and dimensionless shear stress during flood ($\tau_{84}^* = RS/1.65D_{84}$), with R as the hydraulic radius (in m), were used to calculate τ^*/τ_c^* ratios. The Recking (2013a) formula was then used for bedload computation:

$$q_s = \rho_s \sqrt{g(s-1)} D_{84}^3 14 \tau_{84}^* 2.5 / \left[1 + \left(\tau_m^* / \tau_{84}^* \right)^4 \right], \quad (5)$$

with q_s is the bedload-transport rate (in $\text{g s}^{-1} \text{m}^{-1}$), ρ_s the sediment density, g the acceleration of gravity, s the relative density (ρ_s/ρ with ρ the water density), and τ_m^* the transition between full mobility and partial transport given by $\tau_m^* = (5S + 0.06)(D_{84}/D_{50})^{4.4\sqrt{s-1.5}}$ for gravel-bed river. This formula offers a large field application domain (channel slope from 0.00002 to 0.08 m m^{-1} , and D_{84} from 0.9 to

558 mm) and has been successfully tested with a large set of bedload data collected in the field (Recking, 2013b).

5 | RESULTS

5.1 | Flow and bedload transport during the November 2016 flood

Few weeks after the replenishment operation, a large and long-duration Mediterranean autumn flood occurred in the Buëch River (Figure 3a), with a recurrence interval estimated at 5 years at the Serres gauging station. During this flood, EDF carried out a long sluicing operation at the dam (Figure 3b), which encompasses the three flow peaks (Figure 3c). In HUM1 at the peak flow ($265 \text{ m}^3 \text{ s}^{-1}$, November 22, 2016, at 11:00 a.m.), BU1 was submerged, BU2B was in bankfull conditions, and BU2A and BU2C were not submerged (Figure 3d).

Downstream HUM2, flood marks and the mean water depth ($d = 1.23 \text{ m}$) indicate no overflow in the floodplain at the right side of the channel. Maximum specific stream power was estimated at 158 W m^{-2} , and the maximum τ^*/τ_c^* was estimated at 2.43. Total bedload-transport conditions (defined as $\tau^*/\tau_c^* > 2$) concern 25% of the flood duration. The total bedload-transport volume during the

flood was estimated at $12,000 \text{ m}^3$ from hydraulic computation (Figure 3b) with a maximum of $1.611 \text{ kg m}^{-1} \text{ s}^{-1}$ at the peak flow.

5.2 | Bedload travel distances

We obtained a 71% recovery rate of RFID tracers ($n = 105$). Almost all of the recovered tracers were displaced during the period ($n = 100$; 67.5%). Many tracers crossed the dam (19.6%; $n = 29$), whereas others did not (51.4%; $n = 76$). Most of them stopped their course in the alluvial fan (39.2%; $n = 58$). Mobile tracer travel distances range from 12 to 3,406 m, with a mean value of 1,020 m. All the investigated grain sizes have been mobilized during the flood; no grain-size effect on transport distances was observed, and the position along cross section has not influenced travel distances. Frontrunners deposited downstream of the confluence with the Torrent de Channe, in a reach where bedload sheets with avalanche faces were observed just after the flood. The cumulative frequency of transport distances shows that 50% of the tracers travelled a distance greater than 900 m and that a rapid decline of tracer frequency occurs at a transport distance of around 1,700 m (Figure 4). The most mobile tracers were those deployed close to the dam, along Cross Sections 8 and 9, with a mean travel distance of 1,877 m. Tracers deployed far upstream from the dam (Cross Sections 1, 2, 3, and 4) and in the alluvial fan (Cross Sections 5, 6, and 7) showed a mean travel distance of 957 and

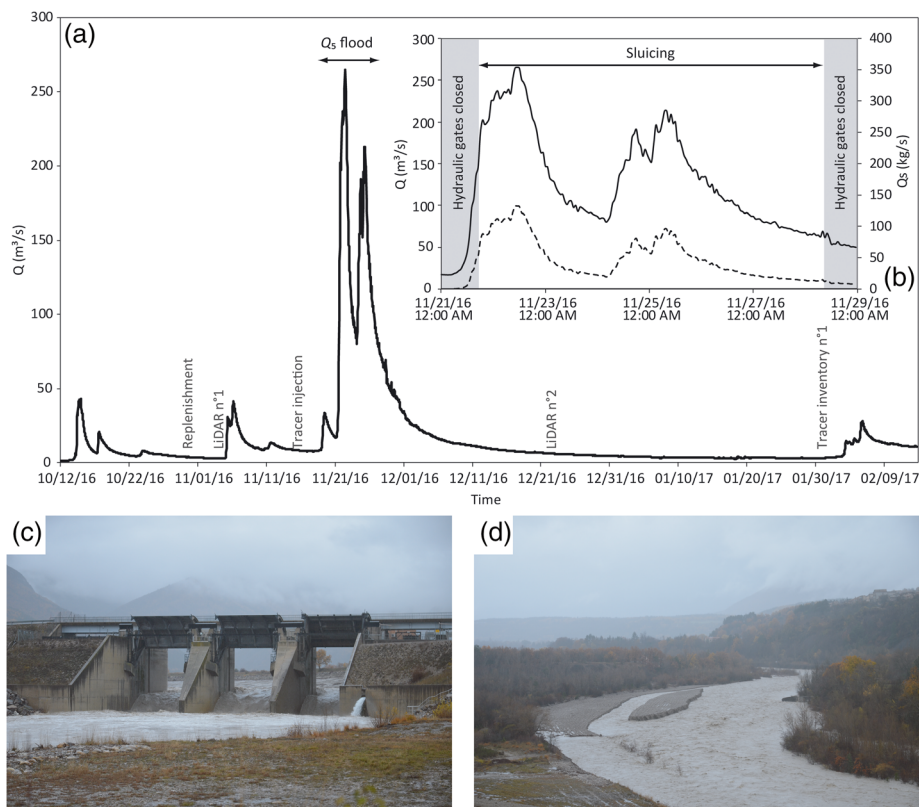


FIGURE 3 Buëch River hydrology during the investigated period. (a) Discharge record at the Serres gauging station. (b) Focus on flood discharge (dark line) and computed bedload transport (dashed line). (c) View of the sluicing operation during the Q_5 flood in November 2016. (d) View of the replenishment site at the time of the peak flow; view looking downstream [Colour figure can be viewed at wileyonlinelibrary.com]

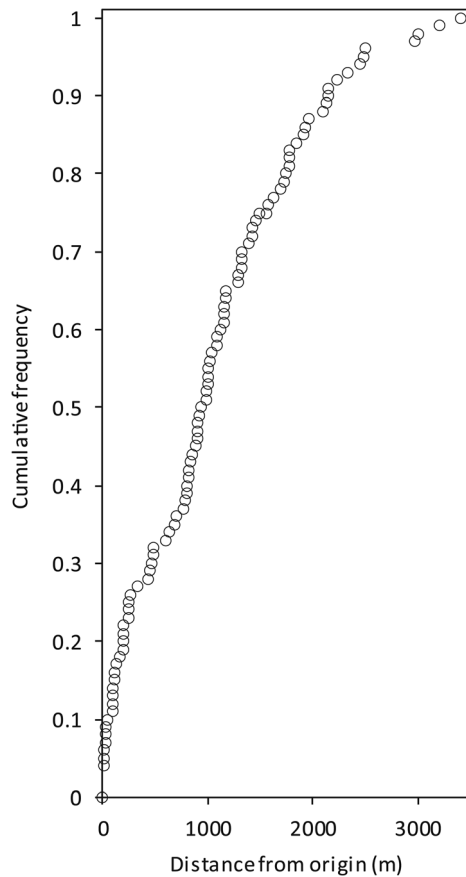


FIGURE 4 Cumulative frequency distribution of radio-frequency identification tracer transport distances during the November 2016 flood

114 m, respectively. Most of the tracers that crossed the dam were injected close to the dam (23/29) on Cross Sections 8 and 9.

5.3 | Sediment remobilization in the replenishment site

In HUM1, the LiDAR-derived DoD shows a gross erosion of $25,450 \text{ m}^3$ ($\pm 40 \text{ m}^3$) and a gross deposition of $7,600 \text{ m}^3$ ($\pm 20 \text{ m}^3$; Figure 5a,b). This negative sediment balance is clearly driven by berm erosion: a PR of 48% was obtained by considering the total volume of berm erosion. The replenishment reach shows a much higher morphological activity in the right side of the channel, where most of the flow was concentrated (Figure 5c,d). Erosion was very important for BU1 ($6,450 \pm 7 \text{ m}^3$) and for BU2C ($14,100 \pm 10 \text{ m}^3$), whereas erosion was very low for BU2A along the trench ($1,550 \pm 2 \text{ m}^3$). PR values obtained for BU1, BU2C, and BU2A are 47.6%, 31.1%, and 85.6%, respectively. Bank erosion of a low terrace accounted for the remaining $2,800 \pm 17 \text{ m}^3$ of sediment loss. A deposit of $800 \pm 2 \text{ m}^3$ was observed along the trench, showing that bedload transport was active in this artificial secondary channel. The remaining $6,800 \pm 18 \text{ m}^3$ of gross deposition are homogeneously distributed over the low-flow channel of the replenishment reach, which exhibits a 0.5-m aggradation after

the flood (Figure 6a). This clearly shows that a significant bedload volume crosses the dam during the flood.

5.4 | Morphological change in the downstream reach

Downstream HUM1, the longitudinal distribution of active-channel bed-level change shows a much higher morphological activity in the first few kilometres downstream of the dam, up to a distance of $\sim 3.5 \text{ km}$, and a lower activity further downstream (Figure 6b). This is a first observation suggesting a strong channel response to sediment replenishment. Along the first 3.5 km downstream of the dam (excepting HUM1), three successive singular reaches can be easily isolated, which alternate in aggradation and degradation. The first one corresponds to a 2-km aggraded reach corresponding to HUM2; the second one corresponds to a 0.45-km degraded reach (upstream part of HUM3, referred to as HUM3a); the third one corresponds to the next 0.75-km aggraded reach (HUM3b).

HUM2 is characterized by a net positive sediment balance ($20,700 \pm 160 \text{ m}^3$; Figure 5a). A general increase of bed level is observed for both Z_{cs} ($\bar{Z}_{cs} = 0.2 \text{ m}$; $\min = -0.3 \text{ m}$; $\max = 0.5 \text{ m}$) and Z_{min} ($\bar{Z}_{min} = 0.5 \text{ m}$; $\min = -0.1 \text{ m}$; $\max = 0.7 \text{ m}$). A downstream gradient of decreasing aggradation intensity is observed along this reach. HUM3a is characterized by a net negative sediment balance ($-4,700 \pm 69 \text{ m}^3$). A decrease of active-channel bed level is observed for both Z_{cs} ($\bar{Z}_{cs} = -0.15 \text{ m}$; $\min = -0.6 \text{ m}$; $\max = 0.1 \text{ m}$) and Z_{min} ($\bar{Z}_{min} = 0.2 \text{ m}$; $\min = -0.9 \text{ m}$; $\max = 0.5 \text{ m}$). HUM3b is characterized by a net positive sediment balance ($10,300 \pm 120 \text{ m}^3$), and an increase of active-channel bed level is observed for both Z_{cs} ($\bar{Z}_{cs} = 0.22 \text{ m}$; $\min = 0.05 \text{ m}$; $\max = 0.6 \text{ m}$) and Z_{min} ($\bar{Z}_{min} = 0.3 \text{ m}$; $\min = -0.2 \text{ m}$; $\max = 0.8 \text{ m}$). Considering the first aggraded unit (HUM2; 2,000 m) or the two others downstream of HUM3 (3,200 m), LR ranges from 5.6 to 8.9.

5.5 | Assessment of the downstream propagation of replenished gravels

The classic sediment balance equation ($O = I - \Delta S$, with O as the sediment output, I the sediment input, and ΔS the net storage change) and the cumulative distribution of tracer transport distances were combined for assessing the downstream propagation of the sediment wave induced by the sediment replenishment operation. By considering sediment loss of the replenishment reach (HUM1), it appears that $25,450 \text{ m}^3$ of gravels has been supplied to the downstream reach of the Buëch River, mainly by lateral erosion of artificial berms ($22,650 \text{ m}^3$). A first way to evaluate the minimum distance at which this volume has been entirely diffused is to look at the cumulative sediment deposition curve downstream of HUM1. This curve shows that the minimum diffusion reach has a length of 2.3 km (Figure 7). By applying the cumulative frequency distribution of tracer transport distances to the volume of berm sediment loss, it is possible to obtain a theoretical curve of the sediment wave deposition. This curve nicely fits to the observed cumulative channel deposition along the first

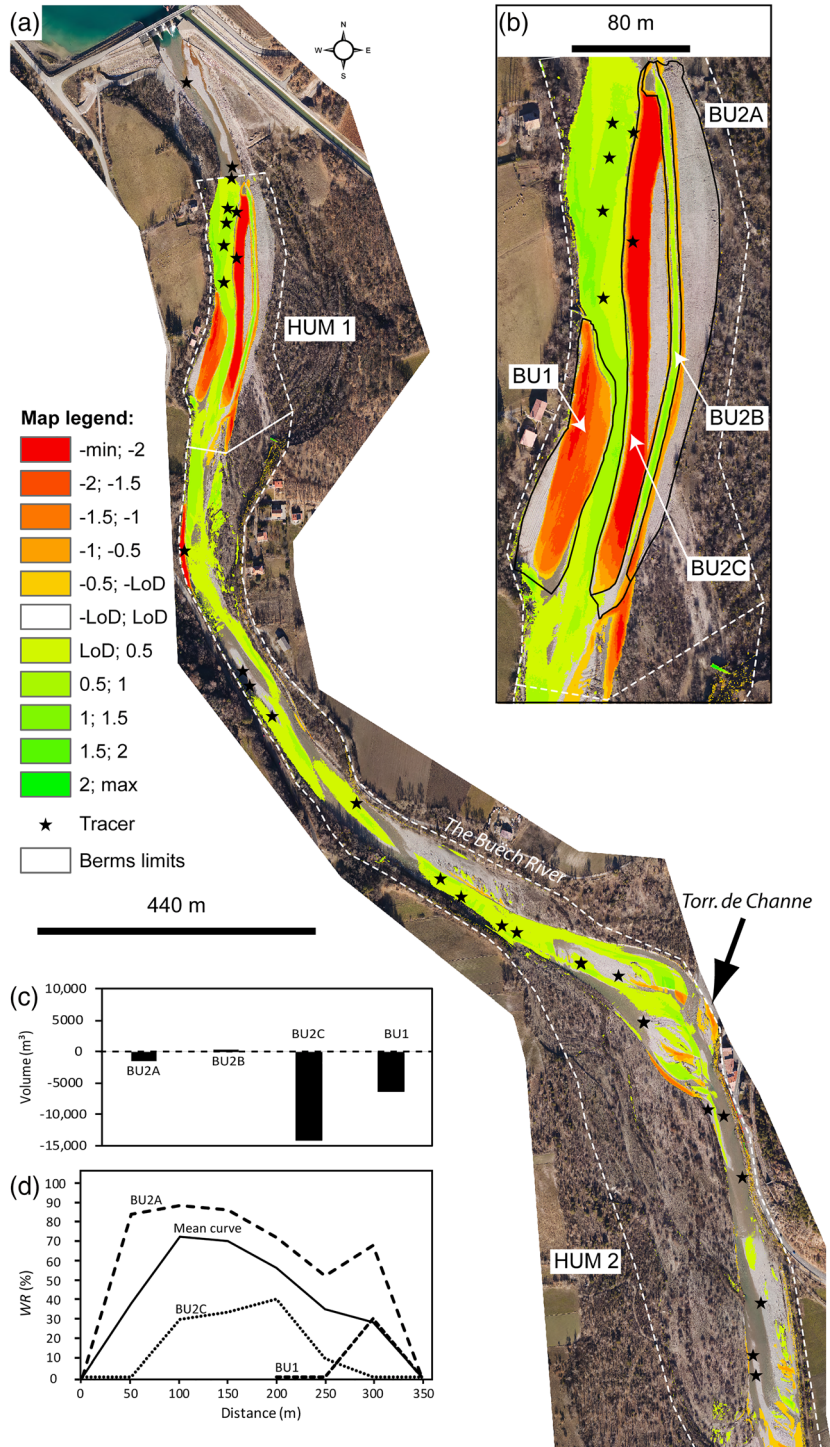


FIGURE 5 Channel change detection map following the November 2016 flood. (a) DoD after LoD subtraction and then exclusion along HUM1 and HUM2; the white dashed lines represent the surface covered by LiDAR data. (b) Zoom-in view of HUM1. (c) Sediment balance for each berm unit (PR). (d) Relative no eroded width ratio (WR). DoD, digital elevation model of difference; LoD, level of detection [Colour figure can be viewed at wileyonlinelibrary.com]

2.3 km of HUM2 (Figure 7). It is likely that this distance of 2.3 km corresponds to the maximum propagation of the sediment wave induced by gravel replenishment. This also means that this distance is likely the appropriate spatial scale to consider for applying a reach-scale sediment balance equation, which is not too biased by sediment throughput.

The application of the sediment balance equation in HUM2 where significant net deposition is observed provides a way to reconstruct sediment transfers of the Buëch River downstream of the dam during the November 2016 flood (Figure 8). The only term of the equation

that has been constrained is the storage change along the reach (net deposition of $20,700 \pm 160 \text{ m}^3$). By considering bedload-transport computation using the flood hydrograph at the downstream end of this reach ($12,000 \text{ m}^3$), it is possible to evaluate bedload inputs at $32,700 \text{ m}^3$. Inputs are divided into (a) berm erosion ($22,650 \text{ m}^3$), (b) bank erosion ($2,800 \text{ m}^3$), and (c) the back-calculated bedload passing through the dam ($7,250 \text{ m}^3$). Because a deposited volume of $7,600 \text{ m}^3$ is observed along HUM1, it should be added to the $7,250 \text{ m}^3$ that passed through to dam, giving a total bedload transport crossing the sluice gates during the flood of $14,850 \text{ m}^3$. This

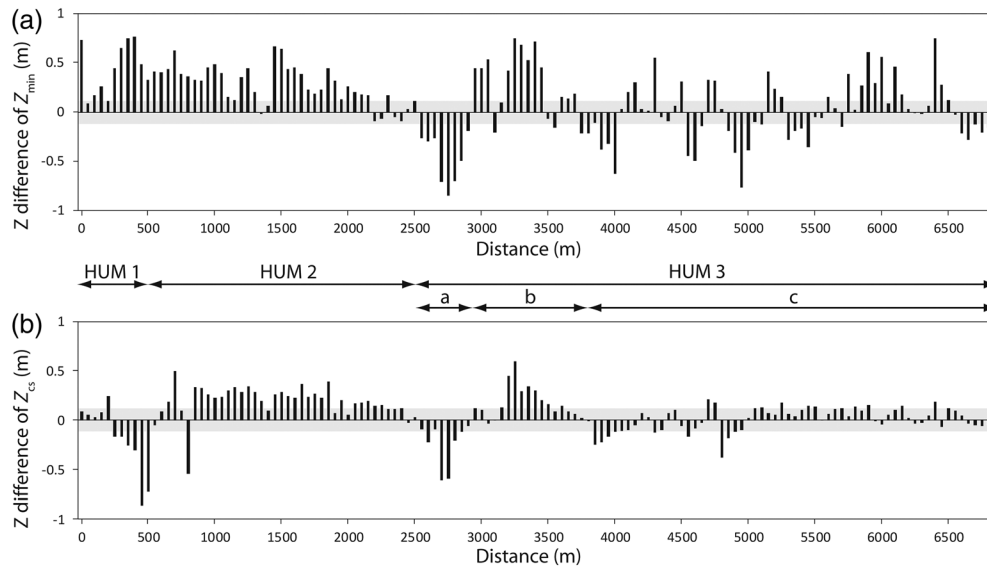


FIGURE 6 Buëch River bed-level change downstream of the dam following the November 2016 flood. (a) Low flow channel evolution (Z_{min}). (b) Active-channel evolution (Z_{cs}). Grey surface corresponds to level of detection

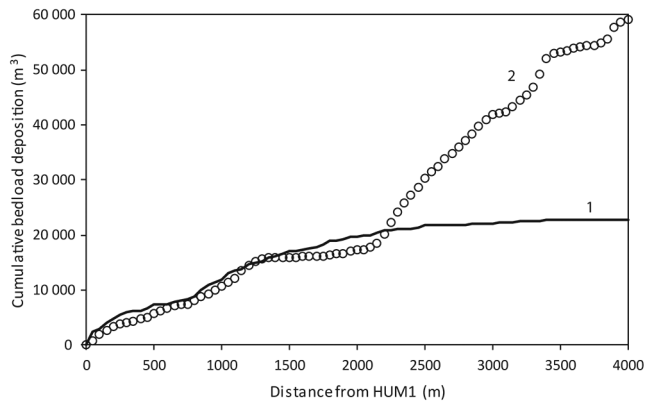


FIGURE 7 Cumulative bedload deposition downstream HUM1. 1: Reconstruction of bedload deposition from tracer CDF. 2: Observed gross deposition using sequential LiDAR surveys

value corresponds to 35% of the mean annual bedload yield upstream of the dam and 74% of the mean bedload yield downstream of the dam.

6 | DISCUSSION

6.1 | How is the downstream propagation of sediment replenishment assessed?

A key issue to consider for the planning of sediment replenishment operations in river channels is the pattern of gravel redistribution downstream of the injection site during flow events. The case of the Buëch River offers a well-documented field experiment where the combination of topographic resurvey covering a long channel reach (~7 km) and bedload tracing successfully helps to isolate the morphological signature of an artificially induced sediment wave.

Both the bed-level evolution and 2D change detection map from sequential LiDAR data reveal a dominant pattern of channel aggradation along a 2.5-km reach downstream of the dam. Further downstream, another sediment deposition zone is observed at a distance of 3.5 km, but this distal aggraded reach is likely not related to the sediment replenishment operation. Additional sediment input from the Torrent de Channe and active channel remobilization could have been deposited in this distal area characterized by a short transition between wandering to braided pattern. The cumulative frequency of bedload-transport distances observed during the flood indeed shows that 90% of the tracers deposited at a distance lower than 2 km. When this cumulative frequency is used to redistribute the effective bedload supply from the replenishment reach, which has been well constrained by sequential LiDAR data, it is possible to reproduce the observed cumulative deposition curve up to a distance of around 2 km downstream of the replenishment reach. Data from RFID tracers clearly help to detect the propagation front of the artificial gravel wave. It should however not be forgotten that the frequency curve of tracers only integrates the coarse fraction of the bedload GSD, and it is possible that the right tail of the distribution is not correctly represented by the observations. This is also supported by the fact that tracers have been deployed upstream of the dam and that their virtual velocity have been potentially reduced by the trapping effect of the dam and its reservoir. A seeding of tracers in the artificial berms would have been better for reconstructing the deposition pattern of the replenished sediment. It is also recognized that a change detection integrating the wet portions of the active channel would have been better for reconstructing the flood sediment balance. However, the fact that the regulated discharge downstream of the dam was strictly the same during the two LiDAR surveys shows that bed-level evolutions obtained for both the active channel and the low-flow channel can be considered as unbiased.

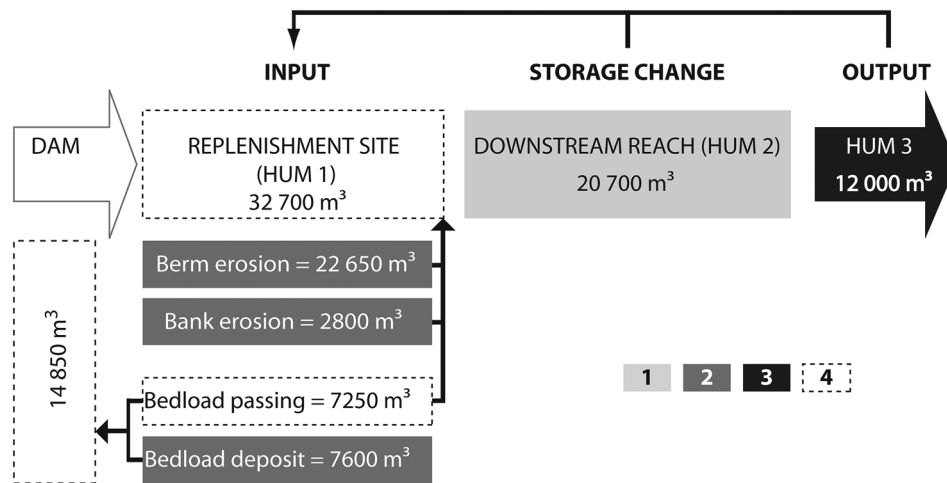


FIGURE 8 Buëch River sediment balance of the November 2016 flood. 1: Net sediment balance from LiDAR surveys. 2: Gross sediment volumes from LiDAR surveys. 3: Bedload calculation. 4: Back-calculated volumes

6.2 | Hydraulic sluicing versus sediment replenishment

Beyond isolating the downstream effect of sediment replenishment, the combination of bedload tracing and topographic monitoring successfully helps to evaluate the respective role of hydraulic sluicing and sediment replenishment in feeding the starved channel reach with sediment. RFID tracers first demonstrated that the sluicing operation during the flood was effective in terms of bedload continuity, because 19.6% of the tracers deployed upstream of the dam have crossed the sluice gates. This is also confirmed by gravel deposition in the channel immediately downstream of the dam, as documented by sequential LiDAR data. The sediment balance calculated for the reach where most of the bedload input from the replenishment site gets deposited also provides a way to back-calculate the total volume of bedload crossing the dam during the flood, provided that the computed bedload export from the investigated reach can be considered as correct. The bedload flux (direct sampling) was not constrained along the reach, because such data are particularly difficult to obtain in the field. Even if some recent advances with seismic sensors deployed along banks have been reported, it is still a challenge to calibrate the seismic signal for obtaining a bedload flux (Burtin, Hovius, & Turowski, 2016). The back-calculated volume represents approximately half of that supplied by the replenishment reach, but only around 25% of the volume crossing the dam effectively contributes to the recharge of the starved channel reach. This clearly shows that hydraulic sluicing alone will be insufficient to stop the channel incision downstream of the dam, and that such operations must be associated with sediment replenishment to compensate the sediment deficit.

6.3 | How efficient is sediment replenishment for feeding starved river channels?

The case of the Buëch River downstream of the Saint-Sauveur dam offered a rare opportunity to document in the field the effect of

artificially built gravel berms in river channels. The high-flow stockpile design of sediment placement into the river channel, which consists of creating artificial berms on each side of the active channel, proved to be a satisfactory approach, because 48% of the replenished volume has been effectively entrained during the first flood following the restoration works. Although this value is far from the maximum theoretical efficiency of 100% entrainment, it is quite similar to maximum values reported for recent sediment replenishment operations in large Alpine gravel-bed rivers (Table 3). The comparison of berm erosion patterns observed for the Buëch River confirms the importance of submergence conditions, as previously demonstrated by flume experiments of sediment replenishment designs (Battisacco et al., 2016). A higher submergence of the berm during flow events should guarantee a better remobilization of the artificially stored sediment. It also appears that the opening of a trench into the berm does not really improve the erosion, likely because the diverted discharge was insufficient to induce significant channel shifting. It is also likely that the trench limited the erosive power of the main channel by diverting a substantial part of the flood discharge. Now, the trench is perched and could not be flooded during high flows.

Efficiency feedback from the Isar River, the Rhine River, and the Buëch River shows the importance of the replenishment volume for sediment balance recovery (Table 3). As shown by deficit recovery rate (DR), it appears that $DR < 20\%$ on the Isar River is not enough for reversing the incision trend. On the contrary, with $DR > 70\%$ on the Rhine River and on the Buëch River, net positive channel storage changes are observed following replenishment. However, maximizing the morphological effects of sediment replenishment depends not only on the reinjected volume but also on the design of berm deployment in the channel. As shown by Battisacco et al. (2016), the comparison of LR values obtained in the Rhine and the Buëch confirms more efficient gravel dispersion when berms are deployed on each side of the active channel. However, it is difficult to conclude about the effect of replenishment design, because differences

TABLE 3 Replenishment feedbacks in large Alpine gravel-bed rivers

Replenishment characteristics	Reference			
	Heckmann et al. (2017)	Steinbock Monument	Arnaud et al. (2017)	This paper
River	Isar River		Rhine River	Buëch River
Site	3rd sill	Steinbock Monument	Kembs	Saint-Sauveur
Drainage area (km ²)	1,138	1,138	34,500	836
Active channel width (m)	80	80	110	70
Replenishment date	2013	2013	2010	2016
Mean annual sediment deficit (<i>D</i> , m ³ year ⁻¹)	10,000	10,000	16,300	20,000
Replenishment volume (<i>R</i> , m ³)	4,010	6,312	23,000	43,500
Design	Single volume	Single volume	Single volume	Parallel volume
Replenishment design	High-flow stockpiles			
Peak flow (m ³ s ⁻¹) of the first flow event after replenishment	150		1,340	265
Flood frequency (<i>Q_f</i>)	0.5		0.5	0.2
PR (%)	60	87	50	48
Effective replenishment (ER, m ³)	1,600	800	11,500	22,650
Deficit recovery rate (DR, %)	16	8	71	113.25
Sediment storage change in restored reach	Erosion	Stability	Deposition	Deposition
LR (m)	-	-	3	5.6

Note. ER = $R(1 - PR)$ and DR = $100 \left(\frac{ER}{D} \right)$.

between sites may be dominated by the size of the replenishment operation (relative to catchment size or active channel width), and by the intensity of the investigated floods, which are both higher for the Buëch. Feedbacks from additional field experiments are still missing to make a comprehensive meta-analysis of design efficiency.

The case of the Buëch River reveals that channel aggradation was not associated with significant channel shifting and active channel widening. The volume effectively entrained along the replenished reach was insufficient to reactivate a braiding pattern along the restored reach and to subsequently increase the downstream effect of the sediment replenishment operation. If channel shifting would have been active in the aggraded reach, the remobilization of low terraces would have contributed to increase the sediment supply and to propagate the morphological restoration along a much longer channel reach. However, the lateral shifting of the aggraded reach would have only been possible downstream of the confluence with the Torrent de Channe, where the active channel is unconstrained by embankments.

7 | CONCLUSIONS

A one-shot major sediment replenishment operation conducted along the dam-impacted Buëch River proved to be successful for reverting channel incision downstream of the dam. Morphological objectives are achieved in a favourable hydrological context and attested for a successful operation.

The complementary use of LiDAR-based topographic resurvey and bedload tracing with UHF active RFID tags successfully helps to

detect the downstream propagation of the sediment wave and to evaluate the respective role of hydraulic sluicing and sediment replenishment in the sediment balance.

In terms of design, some recommendations are also provided to optimize replenishment efficiency in large gravel-bed river: (a) the volume of sediment replenishment should be close to the annual sediment deficit for a significant morphological recovery; (b) the high-flow stockpile design of berm implantation with good submergence is a good solution for maximizing berm erosion; and (c) choice of trench remains uncertain without specific modelling. Beyond design, dam exploitation is a major control factor of efficiency, and sluicing practice should be as frequent as possible in order to maximize sediment balance recovery.

Moreover, monitoring in other hydrological contexts (flash floods with or without sluicing) and a longer survey period will permit to evaluate sustainability of replenishment operation (impact duration, mean residence time of berms, berms fixing, and best frequency for replenishment operation).

ACKNOWLEDGEMENTS

This work benefited from the financial support of the INTERREG Alpine Space HyMoCARES project, Électricité de France (EDF), and Agence française pour la biodiversité (AFB). It has been implemented in the framework of the LTER-ZABR (*Site Atelier Rivières en Tresses*).

ORCID

Guillaume Brousse  <https://orcid.org/0000-0003-1090-1737>

Frédéric Liébault  <https://orcid.org/0000-0002-3155-6779>

Remi Loire  <https://orcid.org/0000-0002-9547-7703>

REFERENCES

- Anderson, S. W. (2019) Uncertainty in quantitative analyses of topographic change: Error propagation and the role of thresholding. *Earth Surface Processes and Landforms*, 44, 1015–1033. <https://doi.org/10.1002/esp.4551>
- Arnaud, F., Piégay, H., Béal, D., Collery, P., Vaudor, L., & Rollet, A.-J. (2017) Monitoring gravel augmentation in a large regulated river and implications for process-based restoration. *Earth Surface Processes and Landforms*, 42, 2147–2166. <https://doi.org/10.1002/esp.4161>
- Astrade, L., Jacob-Rousseau, N., Bravard, J.-P., Allignol, F., & Simac, L. (2011) Detailed chronology of mid-altitude fluvial system response to changing climate and societies at the end of the Little Ice Age (South-western Alps and Cévennes, France). *Geomorphology*, 133, 100–116. <https://doi.org/10.1016/j.geomorph.2011.06.028>
- Battisacco, E., Franca, M. J., & Schleiss, A. J. (2016) Sediment replenishment: Influence of the geometrical configuration on the morphological evolution of channel-bed. *Water Resources Research*, 52, 8879–8894. <https://doi.org/10.1002/2016WR019157>
- Belletti, B., Dufour, S., & Piégay, H. (2013) Regional variability of aquatic pattern in braided reaches (example of the French Rhône basin). *Hydrobiologia*, 712, 25–41. <https://doi.org/10.1007/s10750-012-1279-6>
- Bravard, J.-P., Amoros, C., Pautou, G., Bornette, G., Bournaud, M., Creuzé Des Châtelliers, M., ... Tachet, H. (1997) River incision in South-East France: Morphological phenomena and ecological effects. *Regulated Rivers: Research and Management*, 13, 1–16.
- Burtin, A., Hovius, N., & Turowski, J. M. (2016) Seismic monitoring of torrential and fluvial processes. *Earth Surface Dynamics*, 4, 285–307. <https://doi.org/10.5194/esurf-4-285-2016>
- Carley, J. K., Pasternack, G. B., Wyrick, J. R., Barker, J. R., Bratovich, P. M., Massa, D. A., Reedy, G. D., Johnson, T. R., (2012) Significant decadal channel change 58–67 years post-dam accounting for uncertainty in topographic change detection between contour maps and pointcloud models. *Geomorphology*, 179, 71–88.
- Cassel, M., Dépret, T., & Piégay, H. (2017) Assessment of a new solution for tracking pebbles in rivers based on active RFID. *Earth Surface Processes and Landforms*, 42, 1938–1951. <https://doi.org/10.1002/esp.4152>
- Gautier, E. (1994) Interférence des facteurs anthropiques et naturels dans le processus d'incision sur une rivière alpine - L'exemple du Buëch (Alpes du sud). *Revue de Géographie de Lyon*, 69, 57–62. <https://doi.org/10.3406/geoca.1994.4238>
- Habersack, H., & Piégay, H. (2008) River restoration in the Alps and their surroundings: Past experience and future challenges. In M. Rinaldi, H. Habersack, & H. Piégay (Eds.), *Gravel-bed Rivers 6: From process understanding to the restoration of mountain rivers* (pp. 703–737). Amsterdam: Elsevier.
- Heckmann, T., Haas, F., Abel, J., Rimböck, A., & Becht, M. (2017) Feeding the hungry river: Fluvial morphodynamics and the entrainment of artificially inserted sediment at the dammed river Isar, Eastern Alps, Germany. *Geomorphology*, 291, 128–1442. <https://doi.org/10.1016/j.geomorph.2017.01.025>
- HYDRÉTUDES (2013) Définition d'un plan de gestion des alluvions du Buëch et de ses affluents. Unpublished technical report, SMIGIBA, Aspres-sur-Buëch.
- Juez, C., Battisacco, E., Schleiss, A. J., & Franca, M. J. (2016) Assessment of the performance of numerical modeling in reproducing a replenishment of sediments in a water-worked channel. *Advances in Water Resources*, 92, 10–22. <https://doi.org/10.1016/j.advwatres.2016.03.010>
- Kantouch, S.A., Sumi, T., Kubota, A. & Suzuki, T. (2010) Impacts of sediment replenishment below dams on flow and bed morphology of river. In: *First International Conference on Coastal Zone Management of River Deltas and Low Land Coastlines*, pp. 285–303. Alexandria.
- Kondolf, G. M., Anderson, S., Lave, R., Pagano, L., Merenlender, A., & Bernhardt, E. S. (2007) Two decades of river restoration in California: What can we learn? *Restoration Ecology*, 15(3), 516–523. <https://doi.org/10.1111/j.1526-100X.2007.00247.x>
- Kondolf, G. M., Gao, Y., Annandale, G. W., Morris, G. L., Jiang, E., Zhang, J., ... Yang, C. T. (2014) Sustainable sediment management in reservoirs and regulated rivers: Experiences from five continents. *Earth's Future*, 2(5), 256–280. <https://doi.org/10.1002/2013EF000184>
- Kondolf, G.M. & Minear, J.T. (2004) Coarse sediment augmentation on the Trinity River below Lewiston Dam: Geomorphic perspectives and review of past projects. *Report to the Trinity River Restoration Program*: Weaverville, CA.
- Lallias-Tacon, S., Liébault, F., & Piégay, H. (2014) Step by step error assessment in braided river sediment budget using airborne LiDAR data. *Geomorphology*, 214, 307–323. <https://doi.org/10.1016/j.geomorph.2014.02.014>
- Lane, S. N., Westaway, R. M., & Murray, H. D. (2003) Estimation of erosion and deposition volumes in a large, gravel-bed, braided river using synoptic remote sensing. *Earth Surface Processes and Landforms*, 28(3), 249–271. <https://doi.org/10.1002/esp.483>
- Liébault, F., Gomez, B., Page, M., Marden, M., Peacock, D., Richard, D., & Trotter, C. M. (2005) Land-use change, sediment production and channel response in upland regions. *River Research and Applications*, 21, 739–756. <https://doi.org/10.1002/rra.880>
- Liébault, F., Lallias-Tacon, S., Cassel, M., & Talaska, N. (2013) Long profile responses of Alpine braided rivers in SE France. *River Research and Applications*, 29, 1253–1266. <https://doi.org/10.1002/rra.2615>
- Liébault, F., & Piégay, H. (2002) Causes of 20th century channel narrowing in mountain and piedmont rivers of Southeastern France. *Earth Surface Processes and Landforms*, 27, 425–444. <https://doi.org/10.1002/esp.328>
- Loire R. (2018) Case study: Restoring sediment continuity in the Buëch. *IV Convegno italiano sulla riqualificazione fluviale. Tra cambiamento climatico e consumo di suolo: la riqualificazione fluviale per un nuovo equilibrio del territorio*. Bologna.
- Merz, J. E., Pasternack, G. B., & Wheaton, J. M. (2006) Sediment budget for salmonid spawning habitat rehabilitation in a regulated river. *Geomorphology*, 76(1), 207–228. <https://doi.org/10.1016/j.geomorph.2005.11.004>
- Musashi Y., Nakata Y., Suzuki T., Oshima M. and Demizu S. (2016) A practical example of change of river bed environment downstream from dam reservoir by sediment replenishment, *The 84th Annual Meeting of International Commission on Large Dams*, Johannesburg, South Africa, ISBN 978-0-620-71042-8.
- Ock, G., Sumi, T., & Takemon, Y. (2013) Sediment replenishment to downstream reaches below dams: Implementation perspectives. *Hydrological Research Letters*, 7(3), 54–59. <https://doi.org/10.3178/hrl.7.54>
- Okano, M., Kikui, M., Ishida, H. & Sumi, T. (2004) Reservoir sedimentation management by coarse sediment replenishment below dams. In: *Proceedings of the Ninth International Symposium on River Sedimentation*, pp. 1070–1078. Yichang.
- Piégay, H., Alber, A., Slater, L., Bourdin, L., (2009) Census and typology of braided rivers in the French Alps. *Aquatic Sciences*, 71(3), 371–388. <https://doi.org/10.1007/s00027-009-9220-4>

- Piégay, H., Cassel, M., Dépret, T., Michel, K., & Rollet, A.-J. & Vaudor, L. (2016) Suivi par RFID de la mobilité des galets: Retour sur 10 ans d'expérience en grandes rivières. *Bulletin de la Société géographique de Liège*, 67, 77–91.
- Recking, A. (2013a) A simple method for calculating reach-averaged bedload transport. *Journal of Hydraulic Engineering*, 139, 70–75. [https://doi.org/10.1061/\(ASCE\)HY.1943-7900.0000653](https://doi.org/10.1061/(ASCE)HY.1943-7900.0000653)
- Recking, A. (2013b) An analysis of nonlinearity effects on bed load transport prediction. *Journal of Geophysical Research—Earth Surface*, 118, 1264–1281. <https://doi.org/10.1002/jgrf.20090>
- Recking, A. (2016) A generalized threshold model for computing bed load grain size distribution. *Water Resources Research*, 52, 9274–9289. <https://doi.org/10.1002/2016WR018735>
- Sakurai, T., & Hakoishi, N. (2013) Numerical simulation of sediment supply from dam reservoirs to downstream by the placed sediment. In S. Fukuoka, et al. (Eds.), *Advances in River Sediment Research* (pp. 1193–1199). Taylor & Francis Group, ISBN 978-1-138-00062-9.
- Sklar, L., Fadde, J., Venditti, J., Nelson, P., Wydzga, M., & Cui, Y. (2009) Translation and dispersion of sediment pulses in flume experiments simulating gravel augmentation below dams. *Water Resources Research*, 45(8), 1–14. <https://doi.org/10.1029/2008WR007346>
- Sumi, T. (2006) Reservoir sediment management measures and necessary instrumentation technologies to support them. *The 6th Japan–Taiwan Joint Seminar on Natural Hazard Mitigation*.
- Surian, N., & Rinaldi, M. (2003) Morphological response to river engineering and management in alluvial channels in Italy. *Geomorphology*, 50, 307–326. [https://doi.org/10.1016/S0169-555X\(02\)00219-2](https://doi.org/10.1016/S0169-555X(02)00219-2)
- USDA Forest Service (2004) Gravel mitigation and augmentation below hydroelectric dams. Fort Collins.
- Wheaton, J. M., Pasternack, G. B., & Merz, J. E. (2004) Spawning habitat rehabilitation—II. Using hypothesis development and testing in design, Mokelumne River, California, U.S.A. *International Journal of River Basin Management*, 2(1), 21–37. <https://doi.org/10.1080/15715124.2004.9635219>
- Wolman, G. (1954) A method of sampling coarse river-bed material. *Transactions of the American Geophysical Union*, 35(6), 951–956. <https://doi.org/10.1029/TR035i006p00951>

How to cite this article: Brousse G, Arnaud-Fassetta G, Liébault F, et al. Channel response to sediment replenishment in a large gravel-bed river: The case of the Saint-Sauveur dam in the Buëch River (Southern Alps, France). *River Res Applic.* 2019;1–14. <https://doi.org/10.1002/rra.3527>